

# Towards a deeper understanding of the physics driving galaxy quenching – inferring trends in the gas content via extinction

Joanna M. Piotrowska,<sup>1,2★</sup> Asa F. L. Bluck,<sup>1,2</sup> Roberto Maiolino,<sup>1,2</sup>

Alice Concas<sup>1,2</sup> and Yingjie Peng<sup>3</sup>

<sup>1</sup>*Kavli Institute for Cosmology, University of Cambridge, Madingley Road, Cambridge, CB3 0HA, UK*

<sup>2</sup>*Cavendish Laboratory, Astrophysics Group, University of Cambridge, 9 JJ Thomson Avenue, Cambridge, CB3 0HE, UK*

<sup>3</sup>*Kavli Institute for Astronomy and Astrophysics, Peking University, Yi He Yuan Lu 5, Hai Dian District, Beijing 100871, People's Republic of China*

Accepted XXX. Received YYY; in original form ZZZ

## ABSTRACT

In order to investigate the importance of different proposed quenching mechanisms, we use an indirect method to estimate gas masses for ~62,000 SDSS DR7 galaxies. We infer gas surface densities from dust column densities as traced by extinction within the fibre, applying a metallicity correction to account for varying dust-to-gas ratios. We find that both gas fraction and star formation efficiency (SFE) decrease moving away from the star forming main sequence (MS) towards quiescence for all galaxy masses. We further show that both quantities correlate similarly strongly with the departure from the MS, implying the need for any physical model of quenching to invoke a change in *both* gas fraction and SFE. Our results call for a better understanding of the physical processes driving the decrease in star formation efficiency, which has received relatively little attention in the theory of quenching until now.

**Key words:** keyword1 – keyword2 – keyword3

## 1 INTRODUCTION

Understanding the physical processes responsible for ceasing star formation is one of the long-standing questions in the area of galaxy evolution. Quenching has been shown to correlate well with the total stellar mass of galaxies (e.g. Baldry et al. 2006; Peng et al. 2010), their environment (e.g. van den Bosch et al. 2008; Peng et al. 2012, 2015; Woo et al. 2013; Bluck et al. 2016) and morphology (e.g. Cameron et al. 2009; Bluck et al. 2014, 2019b). A range of phenomena which regulate the gas reservoirs of galaxies were suggested as potential causes of these relations. The processes include gas removal through outflows (e.g. Maiolino et al. 2012; Cicone et al. 2014), or galaxy starvation as a consequence of heating of galactic halos by AGN jets or winds (e.g. Croton et al. 2006; Fabian 2012) or virial shocks (e.g. Dekel & Birnboim 2006; Dekel et al. 2009), as well as gas and halo stripping due to ram pressure exerted on satellites (e.g. Kenney et al. 2004).

Ultimately, galaxies may quench either due to a lack of fuel or a decrease in star formation efficiency (i.e. an increase in the depletion time). To differentiate between these two possibilities we need to measure the dense neutral gas within

galaxies. The most direct probes of gas content are through the observations of the HI 21 cm line and the inference of H<sub>2</sub> masses from observed CO rotational transition lines (see Carilli & Walter 2013 for a review).

Multiple studies have been conducted to measure the neutral gas content in galaxies, including recently Haynes et al. (2018) and Parkash et al. (2018) for HI and Cicone et al. (2017), Saintonge et al. (2017) and Tacconi et al. (2018) for H<sub>2</sub>. However, observing the faint gas emission typically requires long exposure times on premier facilities, thus limiting the sample sizes to only a few hundred detections. Alternatively, less direct methods utilize the far infrared dust emission and empirically calibrated gas-to-dust conversion factors (e.g. Santini et al. 2014; Scoville et al. 2017) to infer gas masses. However, these measurements typically also require multiband data in order to remove the degeneracy between dust mass and temperature, or else rely on assumptions about the latter.

Given that galaxy quenching depends on a range of parameters such as mass, morphology and environment, it is difficult to investigate the subtle interplay of parameters in sample sizes of only a few hundred galaxies. Hence, in order to make progress in understanding the physical drivers of quenching we must find alternative reliable methods of es-

★ E-mail: jmp218@cam.ac.uk

timating gas masses for large galaxy samples, to complement direct detections.

In this work we utilise the correlation between the properties of optical spectra and neutral gas content (e.g., [Bohlin et al. 1978](#); [Concas & Popesso 2019](#)). In our approach, similar to that of, e.g., [Brinchmann et al. \(2013\)](#) and [Barrera-Ballesteros et al. \(2018\)](#), we make use of the attenuation caused by dust to infer gas column densities in the SDSS galaxy spectra. With this method we trade off accuracy for more than a factor of a hundred increase in sample size (i.e. more than 60,000 galaxies). This provides an unprecedented view of the neutral gas content of galaxies in the local Universe.

This letter is structured as follows: in Sections 2 and 3 we describe our sample and gas mass inference method. Section 4 describes our results, followed by discussion in Section 5. We present our summary and conclusions in Section 6.

## 2 DATA AND SAMPLE SELECTION

In our analysis we make use of two publicly available derived data products for the SDSS DR7 ([Abazajian et al. 2009](#)): the MPA-JHU<sup>1</sup> release of spectral measurements and the morphological catalogue of single Sérsic profile fits to photometry by [Simard et al. \(2011\)<sup>2</sup>.](#)

After matching entries from both catalogues we arrive at a total number of 626,062 individual objects, which comprise our parent sample. Each galaxy has an associated in-fibre estimate of star formation rate ([Brinchmann et al. 2004](#)) and stellar mass (following the [Kauffmann et al. 2003](#) approach) along with aperture corrections to total quantities as prescribed by [Salim et al. \(2007\)](#). All objects have a measurement of the  $H\alpha$ ( $\lambda 6563$ ),  $H\beta$ ( $\lambda 4861$ ),  $[O III](\lambda 5007)$ ,  $[N II](\lambda 6584)$  and  $[S II](\lambda \lambda 6717, 6731)$  emission line fluxes, provided by the MPA-JHU release as well. They also have an estimate of the effective radii and bulge ellipticities from the single Sérsic profile fits.

We select our sample by applying the following criteria:

- a galactic disk inclination cut of  $\lesssim 45^\circ$ , which corresponds to an axial ratio cut of  $b/a > 0.7$ ,
- a limit in total stellar mass of  $M_{*,tot} > 10^8 M_\odot$ ,
- S/N cuts of  $> 2$  for  $H\beta$ ,  $> 6$  for  $H\alpha$  and  $> 3$  for  $[O III]$  and  $[N II]$  emission line fluxes

We also remove potential AGN candidates, defined as lying above the [Kewley et al. \(2001\)](#) line in the NII-BPT diagram ([Baldwin et al. 1981](#)). Application of our selection cuts results in 61,158 objects in our final sample with a median redshift of 0.08 and MAD of 0.04.

The inclination cut removes edge-on galaxies, rejecting extremely dust obscured objects due to geometry effects rather than pure dust content. We require an S/N cut on  $H\beta$  and  $H\alpha$  to infer  $E(B - V)$  and our choice of low  $H\beta$  cut aims at striking a balance between accuracy and completeness. Remaining S/N cuts are imposed by our choice of metallicity calibrator. Finally, we remove the AGN sources because they are not likely to sample the dust in the host galaxy, as shown by e.g. [Concas & Popesso \(2019\)](#), since the nebular lines are primarily emitted in the ionisation cones of

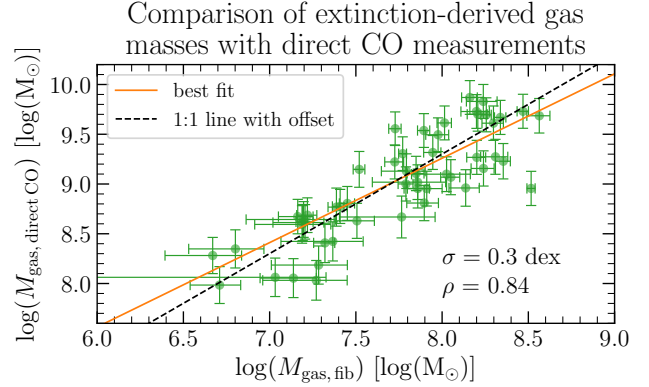


**Figure 1.** Comparison between gas masses obtained from direct CO observations by [Saintonge et al. \(2017\)](#) and this work for 57 matched objects. Horizontal errorbars are result of propagation of uncertainties in fluxes and eq. (2). The values exhibit a linear relation with a best fit plotted as the orange solid line. A unit slope best fit is shown as black dashed line with an intercept value of 1.30. This strong correlation ( $\rho = 0.84$ ) and moderate scatter ( $\sigma = 0.3$  dex) support the use of dust reddening as proxy for estimating the gas content of the SDSS galaxies.

the narrow-line region rather than in the galactic disk. By imposing these selection criteria we preferentially discard the passive sequence, reducing sample completeness to below 10% in this region of the  $M_{*,tot} - SFR_{tot}$  space. Hence, we cannot draw robust conclusions about the passive sequence and restrict our primary discussion to objects ranging from the green valley to starbusts.

## 3 ESTIMATING GAS MASSES

We utilise dust reddening to infer the average column densities of neutral hydrogen from the SDSS optical spectra. More specifically, we use an updated version of an empirical relation between the neutral hydrogen number density and colour excess  $E(B - V)$  ([Bohlin et al. 1978](#)), obtained by [Gudennavar et al. \(2012\)](#):

$$N(H) = (6.12 \pm 0.20) E(B - V) + 0.19 \times 10^{21} \text{ atom cm}^{-2} \text{ mag}^{-1}, \quad (1)$$

where  $E(B - V) = A_V/R_V$  and  $R_V \sim 3.1$  for the Milky Way. This relation was derived in the Galaxy for lines of sight dominated by atomic hydrogen. In our method we assume that the relation extends to total column densities which include regions of dense, molecular phase. We explicitly test this assumption later in this section.

Since equation (1) was derived from observations within the Milky Way, we need to account for the dependence of the dust-to-gas ratio on gas-phase metallicity (e.g. [Issa et al. 1990](#); [Rémy-Ruyer et al. 2014](#)). For this reason we include a metallicity correction in our estimation of gas masses, assuming a linear dependence of the dust-to-gas ratio on the metal content in the gas. In order to implement this correction we estimate metallicity across the entire  $M_{*,tot} - SFR_{tot}$  plane using the O3N2 calibration of nebular emission line ratios extended to non purely star-forming regions by [Kumari et al. \(2019\)](#).

Finally, we make a choice of dust geometry for all objects. We assume an effective foreground screen containing half the total amount of dust in a given galaxy (e.g., [Imara & Blitz 2007](#), [Barrera-Ballesteros et al. 2018](#)). A different

<sup>1</sup> <https://wwwmpa.mpa-garching.mpg.de/SDSS/DR7/>

<sup>2</sup> [ftp://ftp.hia.nrc.gc.ca/pub/users/lsd/astroph/ApJS\\_SDSS\\_2011/](ftp://ftp.hia.nrc.gc.ca/pub/users/lsd/astroph/ApJS_SDSS_2011/)

choice of geometry would influence the conversion factor between the gas mass surface density  $\Sigma_{\text{gas}}$  and  $A_V$ , affecting the quantitative result but not the qualitative trends with other parameters.

Thus, the final relation we use to estimate  $\Sigma_{\text{gas}}$ , assuming a uniform foreground dust screen and linear metallicity dependence in the gas-to-dust ratio, has the form:

$$\Sigma_{\text{gas}} = [(31.6 \pm 1.0)A_V + 1.0](Z_{\odot}/Z) \text{ M}_{\odot}\text{pc}^{-2}. \quad (2)$$

In order to estimate  $A_V$  we compare the observed  $F_{\text{H}\alpha}/F_{\text{H}\beta}$  to its intrinsic Case B value of 2.86 (Hummer & Storey 1987) via the following formula:

$$A_{\lambda} = \frac{K_{\lambda}}{K_{\text{H}\beta} - K_{\text{H}\alpha}} 2.5 \log_{10} \left( \frac{F_{\text{H}\alpha}/F_{\text{H}\beta}}{2.86} \right), \quad (3)$$

where  $K_{\lambda} = A_{\lambda}/A_V$  is taken from any attenuation law of choice. In our study, we choose the parametrisation provided by Cardelli et al. (1989) for a Milky Way attenuation curve of  $R_V \sim 3.1$ , where  $K_V = 1$  by construction,  $K_{\text{H}\alpha} = 0.817$  and  $K_{\text{H}\beta} = 1.164$ . We check that the choice of the attenuation curve does not impact our results by using the Calzetti et al. (2000) curve as an additional test. Although we find small quantitative differences in the resultant gas masses, all trends and hence conclusions are identical. Finally, to obtain a gas mass estimate, we integrate equation (2) over the physical area covered by each 3'' diameter fibre.

In order to validate our indirect method we select objects in our final sample with xCOLDGASS detections (Saintonge et al. 2017) to compare gas masses inferred from reddening with those obtained through CO-to-H<sub>2</sub> conversion. Fig. 1 presents a comparison between the 57 objects present in both samples, which show a strong linear relation with Spearman's rank correlation coefficient of  $\rho = 0.84$ . The in-fibre gas mass estimates are offset to lower values, which is expected because the integrated CO measurements probe the total gas mass in a given galaxy, whereas our approach estimates the in-fibre mass. The best linear fit in the log-log plane (orange solid line) yields a slope of  $0.85 \pm 0.08$  dex and an intercept of  $2.5 \pm 0.6$  dex, while if we fix the slope to unity we obtain an offset of  $1.30 \pm 0.04$  dex with an rms scatter of 0.3 dex around the one-to-one line. This test is encouraging and supports the use of our gas mass estimates to investigate trends in the SDSS DR7 sample.

In order to check whether our main results depend on the choice of calibration we also explored a prescription without the metallicity correction and a preliminary empirical calibration between  $F_{\text{H}\alpha}/F_{\text{H}\beta}$  and  $\Sigma_{\text{gas}}$  from the ALMA-MaNGA QUenching and STar formation survey, (L. Lin et al. in prep.) by Concas et al. (2019, in prep.). We find that all of our main conclusions are preserved, despite some differences in the inferred gas masses of individual galaxies.

## 4 RESULTS

In order to analyse trends with global galactic properties, we compute the gas fraction  $f_{\text{gas}} = M_{\text{gas, fib}}/M_{*, \text{fib}}$  and star formation efficiency  $\text{SFE} = \text{SFR}_{\text{fib}}/M_{\text{gas, fib}} = 1/\tau_{\text{dep}}$ , where the subscript 'fib' denotes in-fibre quantities. The former informs us about the fuel available for star formation while the latter how efficient the gas is at collapsing to form new stars. We focus on the in-fibre quantities, as our gas mass inference is limited to the spectroscopic measurements (i.e. the

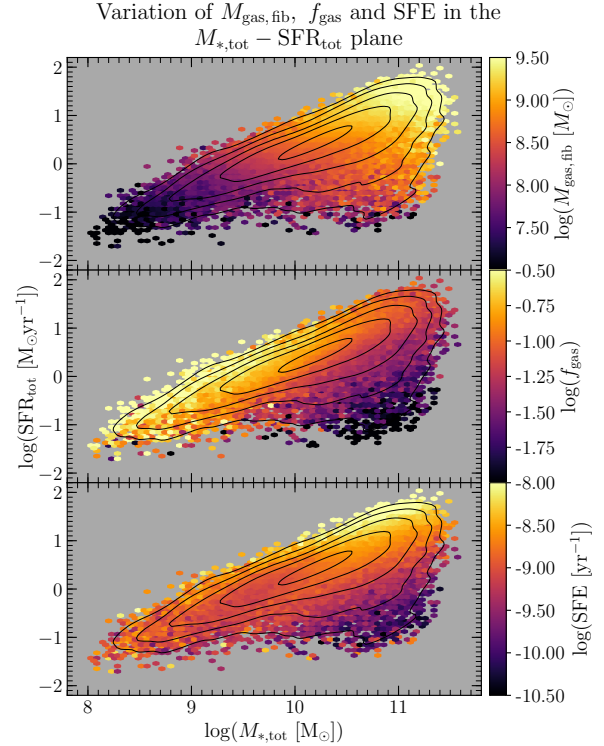


**Figure 2.** Top: in-fibre gas mass ( $M_{\text{gas, fib}}$ ), middle: in-fibre gas fraction ( $f_{\text{gas}}$ ) and bottom: in-fibre star formation efficiency (SFE) variation across the  $M_{*, \text{tot}} - \text{SFR}_{\text{tot}}$  plane, presented in hexagonal bins colour-coded by the median value in each bin. Black contours indicate the number density of galaxies in the plane and are evenly spaced in logarithmic space.

central 3'' of each galaxy). The use of total quantities would require strong assumptions to compute aperture corrections.

In Fig. 2 we present the variation in  $M_{\text{gas, fib}}$  in the top panel;  $f_{\text{gas}}$  in the middle panel and SFE in the bottom panel across the  $M_{*, \text{tot}} - \text{SFR}_{\text{tot}}$  plane. The results are shown in hexagonal bins colour-coded by the median value of each respective quantity. Black contours trace the density of objects in the plane and aid in visualising the distribution of the sample, dominated by the high-SFR objects. Across the Main Sequence (MS),  $M_{\text{gas, fib}}$  shows a smooth increase of  $\sim 3$  dex with increasing total stellar mass, accompanied by a mild decrease in gas fraction and an increase in star formation efficiency. Moving off the MS towards lower SFRs,  $M_{\text{gas, fib}}$  slightly decreases with decreasing  $\text{SFR}_{\text{tot}}$  at constant  $M_{*, \text{tot}}$ , while both  $f_{\text{gas}}$  and SFE show a dramatic drop in values of  $\sim 1$  dex and  $\sim 1.5$  dex, respectively. All quantities also exhibit an increased scatter towards the passive sequence due to the deteriorating statistics.

At a first qualitative glance both  $f_{\text{gas}}$  and SFE show a dramatic variation with increasing deviation from the MS. In order to quantify these trends, we further split our sample into four bins of  $M_{*, \text{tot}}$  and then for each mass bin examine the variation in  $f_{\text{gas}}$  and SFE as a function of deviation from the MS. We define the deviation from the MS ( $\Delta\text{SF}_{\text{MS}}$ ) as distance from the star forming Main Sequence parametrised by a least squares fit to the galaxy sample with  $\text{sSFR} = \text{SFR}/M_{*, \text{tot}} > 10^{-10.8} \text{ yr}^{-1}$  (which excludes the green valley and passive sequence). Our fit broadly agrees with

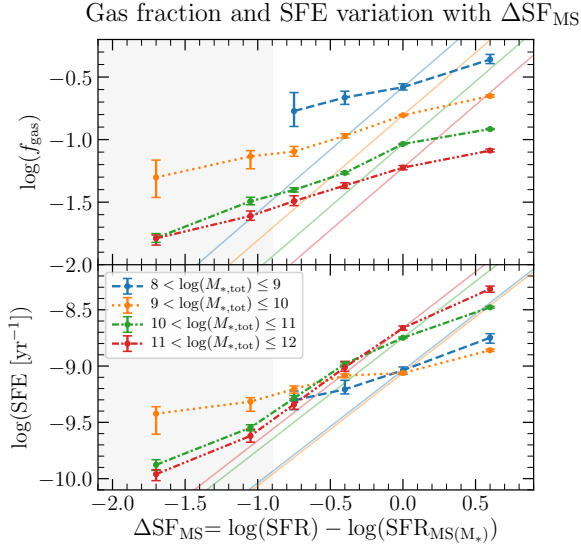


**Figure 3.** Top panel: gas fraction ( $f_{\text{gas}}$ ) and bottom panel: star formation efficiency (SFE) plotted as functions of distance from the MS in four bins of total stellar mass. Each point corresponds to a median value with a bootstrapped error estimate. The grey shaded area covers the range in  $\Delta\text{SF}_{\text{MS}}$  with  $\lesssim 10\%$  completeness in each bin. Both quantities show a clear decrease in value with increasing departure from the MS. The solid lines show the variation in either  $f_{\text{gas}}$  (top panel) or SFE (bottom panel) required to produce the observed variation in  $\Delta\text{SF}_{\text{MS}}$  whilst keeping the other parameter constant. The fact that neither  $f_{\text{gas}}$  nor SFE trace these lines indicates that both parameters correlate with quenching.

the definitions by [Renzini & Peng \(2015\)](#) and [Bluck et al. \(2016\)](#).

Fig. 3 presents  $f_{\text{gas}}$  (top panel) and SFE (bottom panel) varying as functions of  $\Delta\text{SF}_{\text{MS}}$ , where y-values correspond to medians of the given quantity in each  $\Delta\text{SF}_{\text{MS}}$  bin, while x-values indicate the bin centres. Associated 95% confidence bounds on the median are estimated by bootstrapping and presented as vertical error bars. The grey shaded region indicates the range of  $\Delta\text{SF}_{\text{MS}}$  values where the completeness in each bin is lower than 10%.

Both quantities in Fig 3 visibly decrease moving away from the MS towards the quiescent region, and increase moving away in the opposite direction (towards starburst galaxies), for all ranges in  $M_{*,\text{tot}}$ .  $f_{\text{gas}}$  seems to follow similar gradients for all mass bins, while SFE indicates a steeper decrease with decreasing  $\Delta\text{SF}_{\text{MS}}$  in more massive systems than in the less massive ones. The solid coloured lines in Fig. 3 illustrate the variation in  $f_{\text{gas}}$  and SFE required to achieve the variation in  $\Delta\text{SF}_{\text{MS}}$  without variation in the other quantity. That is, we use the identity:  $\text{sSFR} = f_{\text{gas}} \times \text{SFE}$ , fixing SFE to its MS value in the top panel, and  $f_{\text{gas}}$  to its MS value in the bottom panel to obtain the expected variation in the other parameter as a function of  $\Delta\text{SF}_{\text{MS}}$ .

If  $\Delta\text{SF}_{\text{MS}}$  is driven solely by varying quantity A the trends in quantity A would line up with the solid coloured lines and the trends in quantity B would be entirely flat. Fig. 3 shows, however, that neither  $f_{\text{gas}}$  nor SFE is in a perfect agreement with the solid lines, suggesting that both parameters are significantly correlated with deviation from the MS. The Spearman correlation coefficient between  $f_{\text{gas}}$  and  $\Delta\text{SF}_{\text{MS}}$  is 0.44, while between SFE and  $\Delta\text{SF}_{\text{MS}}$  is 0.49.

This result indicates that as we move down towards the passive sequence, *it is not only the gas reservoir of a galaxy which decreases but also the efficiency with which the gas is turned into stars.*

In Fig. 4 we present the variation in  $\Delta\text{SF}_{\text{MS}}$  in the  $f_{\text{gas}} - \text{SFE}$  plane for galaxies with  $M_* > 10^{10} M_{\odot}$ . We can see from the individual galaxy distribution that there is a significant variation in both  $f_{\text{gas}}$  and SFE in the massive part of our sample. The plot illustrates two quenching avenues, showing that in order to move away from the MS at high stellar mass, we need to move towards both lower SFE and lower  $f_{\text{gas}}$  values, deviating fastest when we decrease both quantities by an approximately equal amount. The white arrow points in the ‘quenching direction’ and its inclination angle is calculated following [Bluck et al. \(2019a\)](#), where partial correlation coefficients (PCC) between  $f_{\text{gas}}$  and  $\Delta\text{SF}_{\text{MS}}$  and SFE and  $\Delta\text{SF}_{\text{MS}}$  are treated as vector components of the arrow. The PCC between A and B calculated when controlling for C is given by  $\rho_{\text{AB}|\text{C}}$ :

$$\rho_{\text{AB}|\text{C}} = \frac{\rho_{\text{AB}} - \rho_{\text{AC}} \cdot \rho_{\text{BC}}}{\sqrt{1 - \rho_{\text{AC}}^2} \sqrt{1 - \rho_{\text{BC}}^2}}, \quad (4)$$

where  $\rho_{\text{AB}}$  is a Spearman’s rank correlation coefficient between quantities A and B. The inclination of the arrow is then given by  $\Theta$ :

$$\Theta = \tan^{-1} \left( \frac{\rho_{\text{CB}|\text{A}}}{\rho_{\text{AB}|\text{C}}} \right), \quad (5)$$

where  $\Theta$  is measured from the Y-axis. In Fig. 4  $\Theta \sim 45^\circ$ , as expected from the relationship between  $f_{\text{gas}}$ , SFE and  $\Delta\text{SF}_{\text{MS}}$ . Thus, quenching depend roughly equally on a reduction of gas and an increase in depletion time.

## 5 DISCUSSION

The main conclusion of our analysis is that both  $f_{\text{gas}}$  and SFE decrease with deviation from the Main Sequence, in our selected sample of emission line galaxies. Similar trends to those shown in Fig. 3 are also seen in smaller samples of more direct measurements, including in xCOLDGASS ([Saintonge et al. 2017](#)), PHIBSS ([Tacconi et al. 2018](#)), and ALMA observations of the long wavelength dust continuum ([Scoville et al. 2017](#)). More recently, [Ellison et al. \(2019\)](#) also draw similar conclusions about the importance of SFE in quenching on resolved scales from a sample of 34 galaxies observed with ALMA.

It is important to recognise the caveats associated with our results. First of all, our analysis is limited to the central  $1.5''$  radii (on average  $0.65 \pm 0.25$  of the effective radii) of galaxies sampled by the SDSS fibres. To test whether this impacts our results, we split our sample into narrow redshift bins and repeat the analysis. Although minor quantitative differences are present, all qualitative trends are preserved in each redshift bin. We also check for a tight correlation between the global and in-fibre  $M_*$  and SFR (see Fig. B1 in the online supplementary material) and hence conclude that the fibre aperture is not a source of significant bias in our analysis. We also confirm that our conclusions are identical with respect to the in-fibre MS, as well as the global MS (studied throughout this letter). Additionally, although large, our sample still remains incomplete in the passive sequence, since we require emission line detections for our analysis. As a result, we are biased towards the most gas rich of



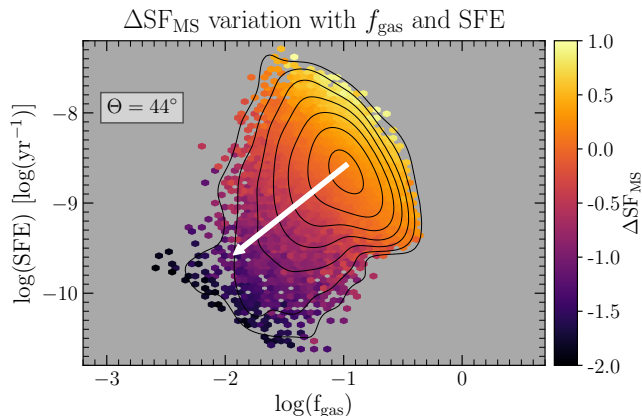


**Figure 4.** Variation of  $\Delta\text{SF}_{\text{MS}}$  in the  $f_{\text{gas}}$ -SFE plane for galaxies with  $M_* > 10^{10} M_{\odot}$ . The colour of each hexagonal bin corresponds to the median value of  $\Delta\text{SF}_{\text{MS}}$ . Black contours indicate number density of objects in the plane.  $\Delta\text{SF}_{\text{MS}}$  becomes increasingly negative as we decrease both  $f_{\text{gas}}$  and SFE. The arrow points in the ‘quenching’ direction, i.e. the steepest gradient in the  $\Delta\text{SF}_{\text{MS}}$  value and is inclined at  $44^\circ$  to the vertical axis.

the passive systems. Consequently, our conclusions are robust throughout the MS and green valley, but are tentative in the passive sequence. Finally, as described in Brinchmann et al. (2013), the assumption of a single attenuation curve for the whole sample is a significant simplification, as this may vary away from the MS (e.g. Salim & Boquien 2019). However, we repeat our analysis with the xCOLDGASS sample (see Fig. A1 in the online supplementary material) and find strong agreement with the trends in Fig. 3. Moreover, these trends are consistent with those found by Tacconi et al. 2018, and thus we are encouraged to conclude that this assumption does not strongly impact our main result.

There is a range of plausible physical mechanisms for decreasing the gas reservoirs available for star formation. One possible channel is the expulsion of gas out of the galaxy in outflows (e.g. Maiolino et al. 2012; Ciccone et al. 2014), which may be driven by AGN or supernovae. Additionally, powerful AGN jets and/or winds may deposit large quantities of energy in the gas halo (e.g. Croton et al. 2006; Fabian 2012), preventing accretion of cold gas through heating. Virial shocks experienced by gas rapidly falling through massive haloes may also be a significant source of heating (e.g. Dekel & Birnboim 2006; Dekel et al. 2009). In these scenarios galaxies quench as a consequence of ‘starvation’, for which there is indirect evidence based on a metallicity analysis of galaxies (e.g. Peng et al. 2015; Trussler et al. 2018). Satellite galaxies are subject to additional environmental effects, including the removal of their dense gas reservoirs by ram pressure stripping (e.g. Kenney et al. 2004) and ‘strangulation’ due to stripping of their hot gas halos (e.g. Peng et al. 2015). The importance of environment to quenching is supported by correlations between quiescence of satellites and local galaxy density (e.g. Peng et al. 2012), satellite location within the group, and the virial halo mass (e.g. Woo et al. 2013).

Varying SFE as a cause of quenching has received less attention in the literature than varying  $f_{\text{gas}}$ . Interstellar turbulence and, to a lesser degree, magnetic fields are proposed as mechanisms regulating star formation (e.g. Federrath &

Klessen 2012), in which case local SFE would depend on the Mach number and the virial parameter of each molecular cloud. Cyclic evolution of the interstellar medium (ISM) between the non-star forming and star forming states could lead to long global gas depletion times in low gas density environments (Semenov et al. 2017), hence potentially linking the decrease in SFE to the decrease in  $f_{\text{gas}}$  (discussed above). Alternatively, the decreased SFE values we observe could be driven by the presence of a prominent bulge, which increases the tidal torques and velocity dispersion within a galaxy, preventing gravitational collapse of the giant molecular clouds. This hypothesis would then link the variation in SFE to galaxy morphology, as suggested by Martig et al. (2009). Finally, the ISM could also be directly heated by energy injection from different forms of AGN activity and stellar winds at different stages of evolution, preventing gravitational collapse and hence decreasing the efficiency of star formation, without significantly reducing  $f_{\text{gas}}$ .

In future work we will attempt to break the degeneracies between the plausible models for quenching outlined above, by utilising the statistical power of our large sample of galaxies with indirect gas mass estimates. More specifically, we will investigate the subtle interplay between mass, morphology, environment and AGN activity in driving variation in  $f_{\text{gas}}$  and SFE.

## 6 CONCLUSIONS

We infer the gas content of  $\sim 62\,000$  local galaxies using the reddening of observed optical spectra in the SDSS DR7. Our choice of indirect method allows for a factor of one hundred increase in sample size compared to more direct methods, trading off accuracy for excellent statistics. When validated against CO observations from Saintonge et al. (2017), our results show a very strong correlation ( $\rho = 0.84$ ) and moderate scatter ( $\sigma = 0.3$  dex) between  $M_{\text{gas, fib}}$  and  $M_{\text{H}_2}$ , encouraging the use of this method for the entire emission line sample of the SDSS.

In this letter we demonstrate that transition towards quiescence results in a significant decrease in *both* gas fraction and star formation efficiency for all galaxy masses, consistent with several previous analyses of much smaller samples utilising more direct gas measurements (e.g. Scoville et al. 2017; Saintonge et al. 2017; Tacconi et al. 2018; Ellison et al. 2019). We further show that deviation from the star forming Main Sequence is similarly strongly correlated with reduction in gas content and lengthening of depletion time. Thus, successful models of quenching must explain both a reduction in gas content and star forming efficiency within transitioning galaxies.

## ACKNOWLEDGEMENTS

We thank the anonymous reviewer for their constructive comments which greatly improved this letter. JMP and YP gratefully acknowledge funding from the MERAC Foundation. AFLB, RM and AC gratefully acknowledge ERC Advanced Grant 695671 ‘QUENCH’, and support from the Science and Technology Facilities Council (STFC). YP acknowledges the National Key R&D Program of China, Grant 2016YFA0400702 and NSFC Grant No. 11773001.

In order to ensure reproducibility, all analysis is publicly available at <https://hub.docker.com/u/jpiotrowska>.

## References

- Abazajian K. N., et al., 2009, *ApJS*, **182**, 543
- Baldry I. K., Balogh M. L., Bower R. G., Glazebrook K., Nichol R. C., Bamford S. P., Budavari T., 2006, *MNRAS*, **373**, 469
- Baldwin J. A., Phillips M. M., Terlevich R., 1981, *PASP*, **93**, 5
- Barrera-Ballesteros J. K., Heckman T., Sánchez S. F., Zakamska N. L., Cleary J., Zhu G., Brinkmann J., and N. D., 2018, *ApJ*, **852**, 74
- Bluck A. F. L., Mendel J. T., Ellison S. L., Moreno J., Simard L., Patton D. R., Starkenburg E., 2014, *MNRAS*, **441**, 599
- Bluck A. F. L., et al., 2016, *MNRAS*, **462**, 2559
- Bluck A. F. L., Maiolino R., Sanchez S., Ellison S., Thorp M., Piotrowska J., Teimoorinia H., Bundy K., 2019a, *MNRAS* in press.
- Bluck A. F. L., et al., 2019b, *MNRAS*, **485**, 666
- Bohlin R. C., Savage B. D., Drake J. F., 1978, *ApJ*, **224**, 132
- Brinchmann J., Charlot S., White S. D. M., Tremonti C., Kauffmann G., Heckman T., Brinkmann J., 2004, *MNRAS*, **351**, 1151
- Brinchmann J., Charlot S., Kauffmann G., Heckman T., White S. D. M., Tremonti C., 2013, *MNRAS*, **432**, 2112
- Calzetti D., Armus L., Bohlin R. C., Kinney A. L., Koornneef J., Storchi-Bergmann T., 2000, *ApJ*, **533**, 682
- Cameron E., Driver S. P., Graham A. W., Liske J., 2009, *ApJ*, **699**, 105
- Cardelli J. A., Clayton G. C., Mathis J. S., 1989, *ApJ*, **345**, 245
- Carilli C. L., Walter F., 2013, *ARA&A*, **51**, 105
- Cicone C., et al., 2014, *A&A*, **562**, A21
- Cicone C., et al., 2017, *A&A*, **604**, A53
- Concas A., Popesso P., 2019, *MNRAS*, **486**, L91
- Croton D. J., et al., 2006, *MNRAS*, **365**, 11
- Dekel A., Birnboim Y., 2006, *MNRAS*, **368**, 2
- Dekel A., et al., 2009, *Nature*, **457**, 451
- Ellison S., et al., 2019, submitted
- Fabian A. C., 2012, *ARA&A*, **50**, 455
- Federrath C., Klessen R. S., 2012, *ApJ*, **761**, 156
- Gudennavar S. B., Bubbly S. G., Preethi K., Murthy J., 2012, *ApJS*, **199**, 8
- Haynes M. P., et al., 2018, *ApJ*, **861**, 49
- Hummer D. G., Storey P. J., 1987, *MNRAS*, **224**, 801
- Imara N., Blitz L., 2007, *ApJ*, **662**, 969
- Issa M. R., MacLaren I., Wolfendale A. W., 1990, *A&A*, **236**, 237
- Kauffmann G., et al., 2003, *MNRAS*, **341**, 33
- Kenney J. D. P., van Gorkom J. H., Vollmer B., 2004, *AJ*, **127**, 3361
- Kewley L. J., Dopita M. A., Sutherland R. S., Heisler C. A., Trevena J., 2001, *ApJ*, **556**, 121
- Kumari N., Maiolino R., Belfiore F., Curti M., 2019, *MNRAS*, **485**, 367
- Maiolino R., et al., 2012, *MNRAS*, **425**, L66
- Martig M., Bournaud F., Teyssier R., Dekel A., 2009, *ApJ*, **707**, 250
- Parkash V., Brown M. J. I., Jarrett T. H., Bonne N. J., 2018, *ApJ*, **864**, 40
- Peng Y., et al., 2010, *ApJ*, **721**, 193
- Peng Y., Lilly S. J., Renzini A., Carollo M., 2012, *ApJ*, **757**, 4
- Peng Y., Maiolino R., Cochrane R., 2015, *Nature*, **521**, 192
- Rémy-Ruyer A., et al., 2014, *A&A*, **563**, A31
- Renzini A., Peng Y.-j., 2015, *ApJ*, **801**, L29
- Saintonge A., et al., 2017, *ApJS*, **233**, 22
- Salim S., Boquien M., 2019, *ApJ*, **872**, 23
- Salim S., et al., 2007, *ApJS*, **173**, 267
- Santini P., et al., 2014, *A&A*, **562**, A30
- Scoville N., et al., 2017, *ApJ*, **837**, 150
- Semenov V. A., Kravtsov A. V., Gnedin N. Y., 2017, *ApJ*, **845**, 133
- Simard L., Mendel J. T., Patton D. R., Ellison S. L., McConnachie

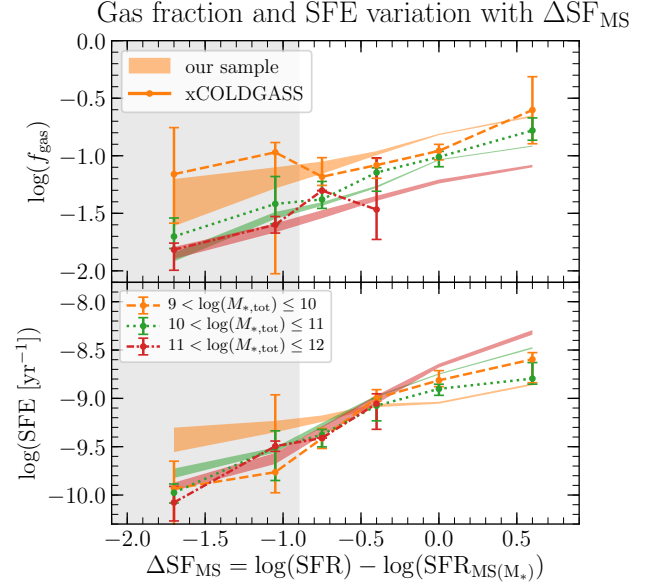


**Figure A1.** Top panel: gas fraction ( $f_{\text{gas}}$ ) and bottom panel: star formation efficiency (SFE) plotted as functions of distance from the MS in bins of total stellar mass. The shaded curves show our data from Fig. 3 in the letter while the solid lines with errorbars are computed using the publicly available xCOLDGASS sample. The two datasets are in a very good agreement with each other, further supporting the conclusions drawn from gas mass inference from optical extinction.

- A. W., 2011, *ApJS*, **196**, 11
- Tacconi L. J., et al., 2018, *ApJ*, **853**, 179
- Trussler J., Maiolino R., Maraston C., Peng Y., Thomas D., Goddard D., Lian J., 2018, arXiv e-prints, [p. arXiv:1811.09283](https://arxiv.org/abs/1811.09283)
- Woo J., et al., 2013, *MNRAS*, **428**, 3306
- van den Bosch F. C., Aquino D., Yang X., Mo H. J., Pasquali A., McIntosh D. H., Weinmann S. M., Kang X., 2008, *MNRAS*, **387**, 79

## APPENDIX A: COMPARISON TO XCOLDGASS

Fig. A1 presents a direct comparison of trends between  $f_{\text{gas}}$ , SFE and  $\Delta\text{SF}_{\text{MS}}$  in the xCOLDGASS and our selected SDSS sample. The SFR and stellar masses used to calculate SFE and  $f_{\text{gas}}$  in both datasets are taken from the MPA-JHU release for consistency and data is binned in the exact same fashion with errors estimated by bootstrapping in each bin. The colours correspond to the different mass bins labelled in Fig. 3 in the letter. Both trends are in a very good agreement with each other. The direct CO measurements show a decrease in  $f_{\text{gas}}$  and SFE as a function of deviation from the MS, supporting our result obtained with a more indirect inference from optical extinction.

The trends in Fig. A1 are also visible in Fig. A2, which presents the two lower panels of Fig. 2 in the letter with 57 matches between our sample and the xCOLDGASS overplotted as coloured circles. Both datasets share the same colourmap for a convenient comparison. The in-fibre inferred quantities (hexagonal bins) are in good agreement with the total ones (circles) within the rms scatter of 0.4 dex presented in Fig. 1 in the letter, showing that the in-fibre analysis does not strongly affect our conclusions.

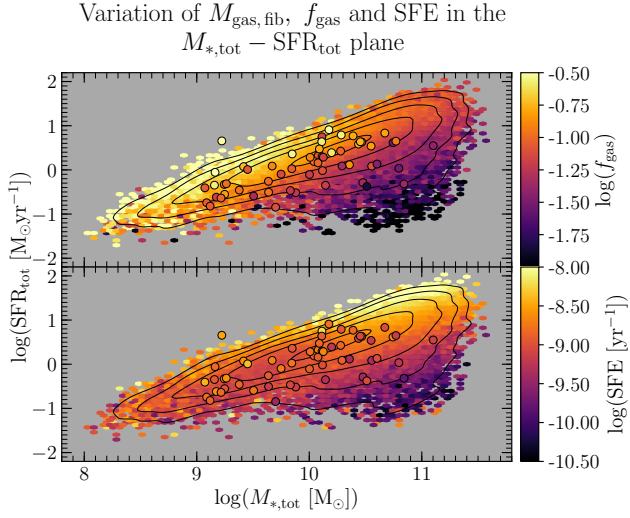


**Figure A2.** Top: gas fraction  $f_{\text{gas}}$ , bottom: star formation efficiency (SFE) variation across the  $M_{*,\text{tot}} - \text{SFR}_{\text{tot}}$  plane. Hexagonal bins present the same data as Fig. 2 in the letter, while coloured circles correspond to the matches between our sample and the xCOLDGASS presented earlier in Fig. 1. Both panels show a good qualitative and quantitative agreement between the fibre-inferred quantities and global measurements based on CO emission.

## APPENDIX B: RELATION BETWEEN THE IN-FIBRE AND GLOBAL QUANTITIES

Fig. B1 further addresses the concern of the influence of a fixed aperture size on the inferred trends. It shows strong correlations between the in-fibre and total quantities within our sample. The Spearman’s rank correlation coefficients of 0.92 and 0.96 as well as small scatter around the linear best fits of 0.23 dex and 0.17 dex for SFR and  $M_*$  respectively show that the in-fibre analysis is a good proxy for the global behaviour of quantities of interest in our study. The trends in Fig. B1 combined with Fig. 1 in the letter suggest that inferred trends in in-fibre  $f_{\text{gas}}$  and SFE should reflect the global ones, as indeed shown in Fig. A1.

This paper has been typeset from a  $\text{\LaTeX}$  file prepared by the author.

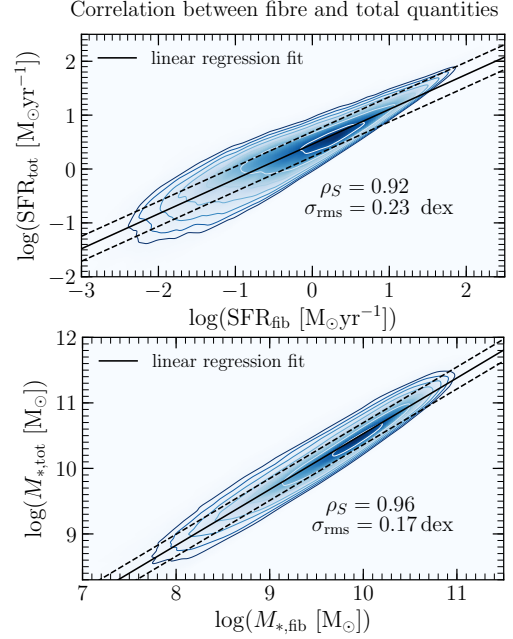


**Figure B1.** Top panel: SFR, bottom panel:  $M_*$  comparison between the in-fibre and total quantities in our sample. The in-fibre estimates for both stellar mass and SFR are very well correlated with the global values with Spearman’s rank correlation coefficients of 0.96 and 0.92 respectively. The relations are also very tight with the corresponding scatter around the best linear fit of 0.23 dex for SFR and 0.17 dex for  $M_*$ .